Upgrade of the Neon Soft X-Ray Spectrometer for Alcator C-Mod

By

Yuri Anatoly Podpaly

Submitted to the Department of Nuclear Science and Engineering
In Partial Fulfillment of the Requirements for the Degree of

Bachelor of Science
In
Nuclear Science and Engineering

June 2007

Accepted by: .....
David G. Cory
Professor of Nuclear Science and Engineering
Chairman, NSE Committee for Undergraduate Students

Approved by: .....
Ian Hutchinson
Professor of Nuclear Science and Engineering
Thesis Supervisor

Approved by: .....
John Rice
Principal Research Scientist
Research Advisor

Author: .....
Department of Nuclear Engineering
May 18, 2007

Upgrade of the Neon Soft X-Ray Spectrometer for Alcator C-Mod

by

Yuri Anatoly Podpaly

Submitted to the Department of Nuclear Science and Engineering on May 18, 2007
In Partial Fulfillment of the Requirements for the Degree of
Bachelor of Science in Nuclear Science and Engineering

Abstract

In order to study plasma rotation, temperature, and impurity density, a Neon Soft X-ray Spectrometer (NeSoXs) was installed on the Alcator C-Mod tokamak. This spectrometer used a spherically bent mica crystal as the reflective element in order to separate the spectral and spatial information on the receiving CCD. The original NeSoXs was found to have several problems including vacuum quality, camera readout rate, crystal positioning, chamber size, and chamber positioning. In order to remedy these problems, a new system was designed and has been constructed. This system has achieved much better vacuum pumping times (~100 times faster) and is in the process of being installed on the Alcator C-Mod vessel.

Thesis Supervisor: Ian Hutchinson
Title: Professor of Nuclear Science and Engineering

Blank Page

2. Table of Contents

3. List of Figures

4. Acknowledgements

I would like to express my deepest gratitude to several people for their help and support of my thesis work and undergraduate career in general. First, I would like to thank John Rice whose serendipitous encounter with my first year advisor led to my joining the Alcator C-Mod project, and who provided me with advice and help throughout the last three years. I owe a great deal of gratitude as well to Alex Ince-Cushman who initiated the NeSoXs project and has supported me with his assistance and advice since the summer of my freshman year. I am also grateful for the privilege of working with Professor Ian Hutchinson who agreed to advise this thesis and helped me with many organizational issues that arose. It has been a great pleasure working with Manfred Bitter and Sanggon Lee, who constructed NeSoXs I and assisted in the calibration and repair of NeSoXs II. Matt Reinke, Aaron Bader, and Ken Marr also helped me with the many technical issues that arose during this project. I would also like to thank the entire Alcator C-Mod staff for their expertise and assistance. Last but certainly not least, I would like to express my gratitude to my family for encouraging me to attend MIT and for their help, advice, and support that is far too numerous to list.

5. Introduction

In recent years, power generation has become a very important issue in public policy and in the research world. With many political and economic issues arising from oil and natural gas power sources and the limited extent to which hydroelectric and solar generators can be used, nuclear power is becoming more appealing. With many problems that affect current commercial power plants, such as fuel procurement, closing the nuclear fuel cycle, and nuclear waste storage, fission power has reached a temporary impasse in the United States of America. This makes the other possible nuclear power alternative, fusion energy, more attractive. Fusion, which is currently in its infant stage of development, has the potential to provide a clean, efficient, and abundant source of power.

Fusion reactions require high temperature to occur and high density to be cost effective. There are two primary methods of creating controlled terrestrial fusion reactions: inertial confinement and magnetic confinement. In inertial confinement, the required density and temperature are obtained by using powerful lasers to implode small pellets of hydrogen. Magnetic confinement uses magnetic fields to limit the plasma diffusion to the walls of the confining chamber. In the early days of fusion research, experiments were conducted on linear machines with field lines ending on material walls. These machines suffered major particle losses, leading A. D. Sakharov and I. E. Tamm to design the tokamak (anagram of translation from Russian "**то**роидальная **ка**мера в **маг**нитных **ка**тушках"), a toroidal chamber with closed magnetic fields confining the plasma. In a tokamak, a central magnetic coil is used to heat the plasma Ohmically. The plasma resistance, η, is given approximately by

$$\eta = \frac{\pi e^2 m^{1/2}}{(4\pi\varepsilon_0)^2 (KT_e)^{3/2}} \ln\Lambda, \qquad (1)$$

where m is the ion mass, K is Boltzmann's constant, ε_0 is the permittivity of free space, ln Λ is approximately 15, and T_e is the electron temperature. From this equation, it is seen that the resistance is inversely proportional to the electron temperature raised to the 3/2 power. Therefore, Ohmic heating is only effective for temperatures up to a few keV. To heat the plasma further, either neutral beam or wave heating is used. The beam method uses a beam of neutral particles to dissipate its energy in the plasma. Another method that has been mentioned as a future possible heating method is alpha particle (He^{++}) heating. The wave heating methods inject microwave radiation at various resonant frequencies of the targeted plasma, which excites the ions or electrons and energizes the plasma.

The following project was completed entirely on the Alcator C-Mod tokamak at the MIT Plasma Science and Fusion center. The Alcator C-Mod tokamak is a compact high field, magnetically confined fusion device with a major radius of .67 m and a minor radius of .21 m, and it is capable of running plasmas with a toroidal magnetic field, B_0, of 8 Tesla and a plasma current, I_p, of 2 MA [1]. A temperature cross section contour plot of the plasma is shown in Figure 1. Alcator has both Ohmic and Ion Cyclotron Range of Frequencies (ICRF) auxiliary heating. Recently a wave based heating and current drive system, which focuses on the Lower Hybrid resonant frequency, has been installed. Typical Alcator discharges tend to run for two seconds with a magnetic field strength of 5.4 Tesla on axis and plasma currents of 1 MA. Alcator also has two general confinement modes, which are called L-mode (low energy confinement), and H-mode (high-energy confinement). In H-mode, which was discovered in 1981 on the ASDEX machine [2], the plasma stored energy and density rise, with density and temperature forming a steep gradient region at the plasma edge. The reason for increased energy

confinement in H-mode is a complex one and is not fully understood. Neo-classical theory predicts energy confinement that is much better than what is measured experimentally. This poor confinement is caused by turbulence in the plasma. When an H-mode forms, there are strong velocity gradients at the plasma edge that tend to suppress the turbulence and decrease the diffusion of energy, improving confinement.

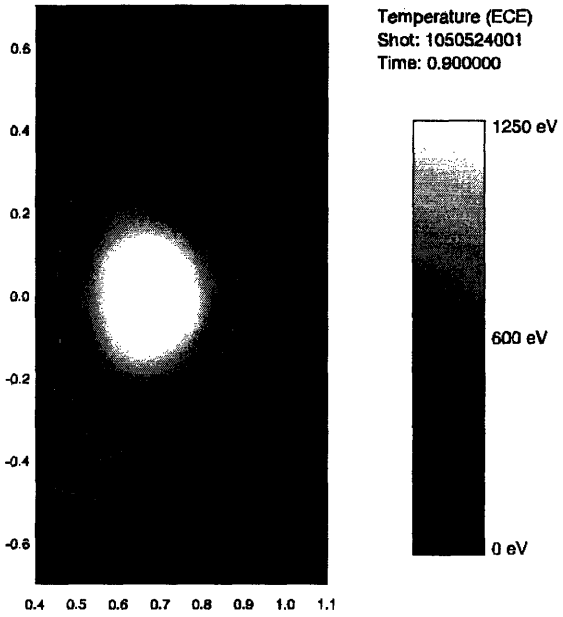

Figure 1. Alcator C-Mod temperature and plasma cross-section. Separatrix is shown as a dotted line.

Given the importance of plasma rotation, temperature, and density, a wide assortment of spectrometers have been installed on Alcator to measure these plasma parameters. They include the ECE, Thomson scattering, and HiReX diagnostics, each measuring different characteristics of the plasma with different physical analysis methods. The high resolution X-ray spectrometer (HiReX) is of particular interest to this experiment; it uses a quartz crystal to separate the wavelength components of the income radiation. HiReX is capable of using the emission lines of hydrogen-like and helium-like argon from the plasma to measure the argon density, ion-temperature, and rotation velocity. These values are found by measuring the emission line

intensity, width, and Doppler shift, respectively. The HiReX spectrometer arrays have tangentially viewing ports into the plasma. The design allows each spectrometer to measure one tangential chord of the plasma. Recently a new HiReX spectrometer, called HiReX Spatial Resolution (HiReX SR), has been installed on Alcator with the ability to image the entire plasma.

The Neon Soft X-ray spectrometer, dubbed NeSoXs, uses a spherically bent mica crystal to allow a single CCD camera to collect spectral and spatial information. The arrangement of the crystal was designed to measure the helium-like neon emission lines. The spectrometer consists of a spherically bent mica crystal as the dispersive element, an aluminum filter to remove visible light, and an X-ray sensitive CCD as the detector. These components are arranged in the Johann configuration [3] in which a single CCD camera can analyze the location, the intensity, and the wavelength of the incident X-rays. Using the methods described in [4], these parameters can provide spatially resolved density, velocity, and temperature measurements of the neon impurity. Furthermore, by taking multiple readouts per discharge, it is possible to track temporal changes in the emissions from the plasmas. The device was originally designed for use on the Hanbit mirror machine [5, 6].

The Neon Soft X-ray spectrometer was tested on Alcator, and it proved successful in obtaining data. Due to problems with the housing design, camera acquisition rate, and spectrometer view of the plasma, NeSoXs was unable to measure the Doppler shift and achieve a poloidal rotation measurement. The redesign of the spectrometer was planned on a better plasma-viewing window. The opportunity to move and redesign the spectrometer was used to build it

with a movable support, rotatable crystal, better vacuum isolation, and a camera with higher resolution.

6. Theoretical Background

The theory behind the spectrometer and its redesign is based on standard plasma interactions and bent crystal spectroscopy. First, plasmas are ionized gases where the ions and electrons can be treated as separate species. Depending on the temperature, however, the ionization is not always complete and non-fully stripped atoms remain. Bound electrons in the non-fully stripped ions can be excited to higher energy via radiative or collisional methods and then de-excite producing measurable X-rays. Free electrons, also, can recombine with the fully and non-fully stripped ions, producing X-rays. Second, many spectrometers use a Bragg reflection off a crystal lattice to separate X-rays based on their wavelength. By altering the geometry of this crystal and focusing the beam, several useful effects can be achieved.

a. Plasma Interactions

i. Radiation from Bound Electrons

The electromagnetic radiation from bound electrons takes the form of a narrow spectral line. These narrow lines occur due to the quantum nature of the electron shells: atoms have finite number of electrons that can occupy a finite number of shells. The energy of the shells is based on their quantum number with some splitting occurring from the spin orbit coupling of the shells and some other small effects. Electrons can only transition between these finite levels, so their energies are bound, and if a transition occurs, it will have a finite range of energies at which it can occur. For instance, the approximate energy equation for the transitions in hydrogen is given as:

$$E_{nn'} = -13.6\left(\frac{1}{n^2} - \frac{1}{n'^2}\right)eV. \tag{2}$$

$E_{nn'}$ is the energy difference required by the transition, and the values n and n' are the initial and final state of the electron in the transition.

There are three processes for radiative transitions in plasma: spontaneous electron decay from an upper energy level, absorption of a photon causing a rise to a higher level, and radiation-induced decay. These transitions have governing equations and associated probabilities denoted by A_{ij}, B_{ij}, and B_{ji} known as the Einstein coefficients for the transition. The probability of spontaneous decay is A_{ij}, which is defined as

$$A_{ij} = \frac{8\pi h \nu_{ij}^3}{c^3} B_{ij}. \tag{3}$$

The radiation induced decay constant is

$$B_{ji} = \frac{g_i}{g_j} B_{ij}, \tag{4}$$

where g_i is the number of states in level i.

The final transition probability, photon absorption, is

$$B_{ij} = \frac{1}{g_i} \frac{8\pi^3}{3h^2(4\pi\varepsilon_0)} S_{ij}, \tag{5}$$

where h is Planck's constant, ε_0 is the permeability of free space, and S_{ij} is the spectroscopy line strength. S_{ij} is defined as

$$S_{ij} = \left| \int \psi_i e\mathbf{r} \psi_j^* d^3\mathbf{r} \right|^2, \tag{6}$$

where ψ_i is the electron wavefunction in the state i (these can be referenced in standard quantum mechanics textbooks see [7]), and **r** is the position vector for the state.

Besides the radiative processes, there are collisional methods of exciting electrons into upper energy levels, after which they decay with energies described by equation 2. These processes are electron impact excitation or deexcitation, impact ionization, and dielectronc recombination. The first two processes are similar to the radiative transitions between bound states and free-bound electron transitions; the collisional excitation simply changes the method for raising the electron to a higher level. Dielectronic recombination is the process of capturing a free electron and using the electrons excess energy to excite a lower level bound electron. [4]

Collisional processes are governed by a reaction's microscopic cross section $\sigma_{ij}(\upsilon)$. The total interaction rate is the macroscopic cross section, $n_i\,\sigma_{ij}(\upsilon)$, times the velocity, υ. This average rate is described as

$$n_e\langle\sigma_{ij}v\rangle = \int \sigma_{ij} f(v) v d^3v \,. \qquad (7)$$

By combining all of these parameters, probabilities can be found that determine the emission rates from the plasma. Emission information is found theoretically and empirically for atoms that are more complex; this information provides great insight on where the emitting elements are located and their current state.

ii. Information in Emission Lines

Each line in a spectrum contains a wealth of information. The intensity of a line provides an estimate of the ion density, which is important for plasma impurity studies. Furthermore, ionization of elements happens at different temperatures. Therefore, by finding where in the plasma certain species are localized, one can estimate the temperature distribution in the plasma itself.

The second important aspect is the line width, which is a measure of how much the theoretically discrete in energy emissions from atoms spread out. Doppler and plasma pressure,

negligible for the X-ray spectroscopy described later, effects cause this spreading. Both of these are related to the temperature of the plasma ion temperature, and so the width of the spectrum gives a measure of plasma temperature.

Further information is contained in the line shift due to the rotation of the plasma. The velocity of the emitting ions compresses or expands the wavelength of the emitted radiation, so the shift of the emission line from the known wavelength can be used to find the velocity of the ions. Heavier ion emissions tend to provide better information about the ion flow velocities, but because of their poor confinement characteristics, their number in tokamaks is often actively minimized [8].

iii. Neon and Alcator C-Mod

The NeSoXs device is designed to measure the emissions from the $1s^1 2p^1 \rightarrow 1s^2$ transitions in helium-like neon. In order for this system to function, neon is injected into the Alcator chamber through a gas valve. The relative amounts of each of the ionization levels of neon depend on temperature of the plasma, and these are shown in Figure 2.

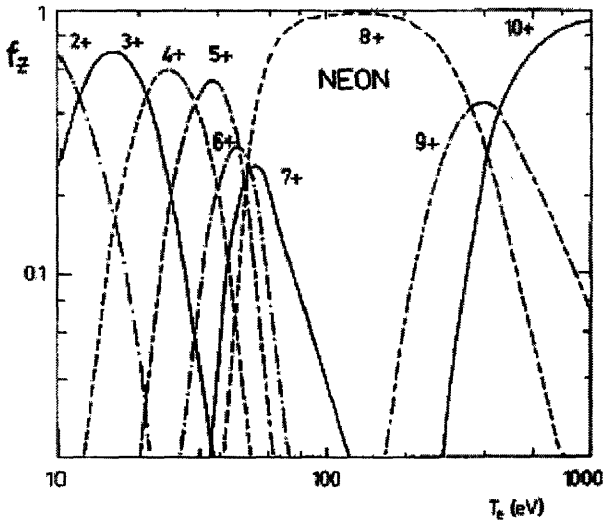

Figure 2. The fractional abundance of charge states of neon depending on the temperature. [6].

Using the emissivity constants and the Multiple Ionization State Transport (MIST) codes for neon, it is possible to find where the impurity will be localized and thus where the greatest emission will occur. [9] In Figure 3, the calculated location of the 2p→1s He-like neon emission line is shown.

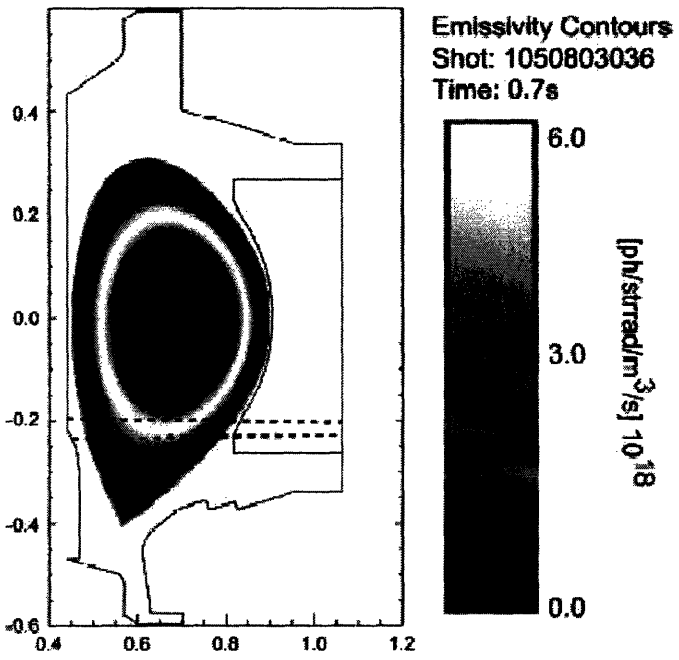

Figure 3. Emissivity profile for helium-like neon in an Alcator discharge. The black dotted lines show the line of sight of the original NeSoXs. [10]

At the center of the plasma, the temperature is too great for helium-like neon to exist, so the emissivity profile is hollow. At the outermost edge of the plasma, the temperatures fall off and the prevalence of the species falls as well.

The primary neon line is located at 1.35534 nm, which intercombination line Y. There are, however, several neon satellite lines between 1.35 nm and 1.38 nm, due to the different spin

states neon and their interactions. In addition, there are several other impurities that radiate in this spectral regime, some of which are shown in Figure 4.

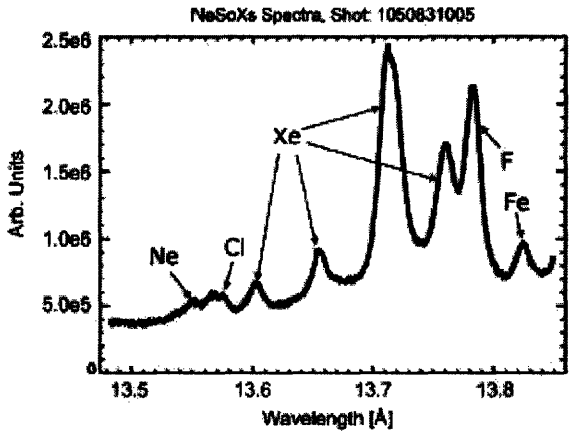

Figure 4. Emissions from the fifth Alcator plasma discharge on August 31, 2007. This discharge shows a wide variety of impurities in the plasma. [10]

iv. Final Notes

The Neon Soft X-ray spectrometer was intended to be able to measure the poloidal rotation profile in the plasma, given helium-like neon's occurrence at the edge of the plasma and the spectrometer's edge viewing geometry. This measurement was sought because of the relationship between poloidal rotation and the edge electric field, which is important in H-mode formation and, thus, fusion energy as a whole [11].

b. Bent Crystal Spectroscopy

i. Bragg Reflection

The basic physical principle of bent crystal spectroscopy is Bragg reflection. Bragg reflection is the process by which electromagnetic waves are reflected from an ordinary patterned lattice. Since a wave is made up of photons, and each photon can be reflected from a separate plane of the crystal lattice, constructive interference will only occur for certain angles of reflection. Figure 5 depicts this reflection from the planes of the crystal, and the extra phase shift

that is gained because of the excess distance traveled by the waves reflected by lower lattice planes.

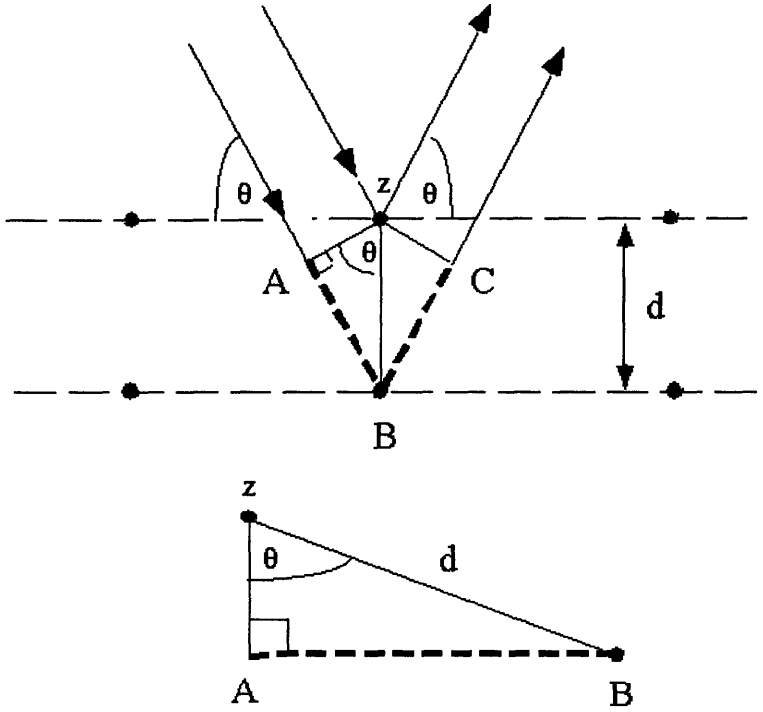

Figure 5. Schematic of Bragg reflection. [12]

As seen in the figure above, constructive interference will only occur when the distance traveled by X-rays striking different lattice planes is an integral multiple of their wavelength. Expressed otherwise, constructive interference occurs when

$$n\lambda = 2d\sin(\theta), \tag{8}$$

where n is an integer, λ is the wavelength of the wave, d is the lattice spacing, and θ is the Bragg angle. The value λ is directly related to the energy of the wave since

$$E = h\upsilon = \frac{hc}{\lambda}, \tag{9}$$

where h is Planck's constant, c is the speed of light, and υ is the frequency of the wave.

ii. Bent Crystals

A crystal that is curved in one of the directions normal to its reflecting face gains several useful characteristics. For instance, a singly bent crystal can focus the different wavelengths of light to a single point at a given distance. The Neon Soft X-ray spectrometer uses a spherically bent crystal, which, because of the Bragg reflection depending on the angle of incidence in two dimensions and the energy of the photon, has the property of separating the spatial component of the X-rays in the vertical direction and the spectral component in the horizontal direction. The NeSoXs crystal is bent with equal radii vertically and horizontally, at a radius of 1524 mm. The crystal is 70 mm wide and 17 mm high, and it has a 2d spacing of 1.99 nm.

iii. The Johann Configuration

The basis of this diagnostic is the Johann arrangement for spherically bent crystal spectrometers. This arrangement was invented in 1931 [13], and it is a configuration for a source, spherically bent crystal, and detector in order to maximize the resolution at the detector. This is shown in Figure 6, with the source replaced by an X-ray tube.

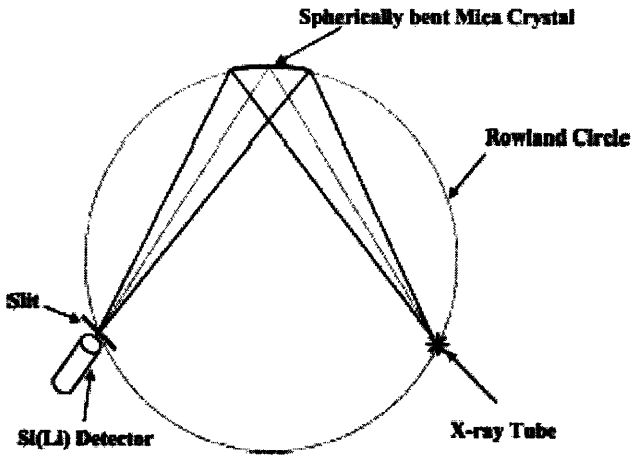

Figure 6. The arrangement of the crystal, source, and detector in the Johann geometry. [14]

The Rowland circle has a radius of half the curvature of the bend in the crystal. At these distances, the rays from the source and to the detector are at focus points. Figure 7 shows a generalized form of the Johann configuration with an extended plasma source.

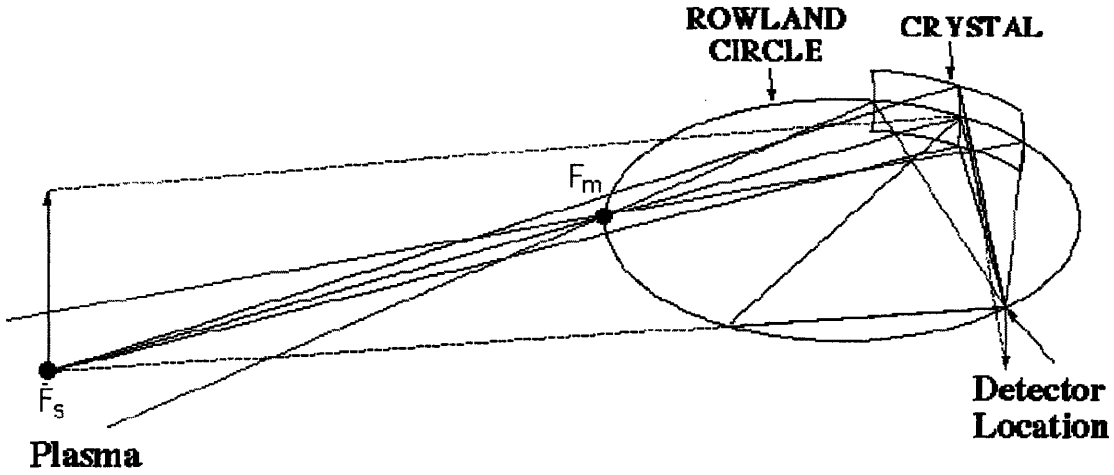

Figure 7. Generalized ray trace for a Johann configuration spectrometer. [15]

In Figure 7, the points f_m and f_s are related by the equation

$$f_s = -f_m / \cos(2\theta), \tag{10}$$

where $f_m = R_c \sin(\theta)$, R_c is the curvature of the crystal, and θ is the Bragg angle of the crystal. As seen in Figure 7, the vertical component of the lines, the spatial information for NeSoXs, is focused at f_s, which is outside the Rowland circle, while the horizontal component, the spectral information, is focused at f_m on the Rowland circle. The width of the detector follows the horizontal component of the reflection from the lines, while the trace of the height of the detector is spread out by the crystal diffraction at 1.5°. Figure 8 shows the spatial spread of the detector.

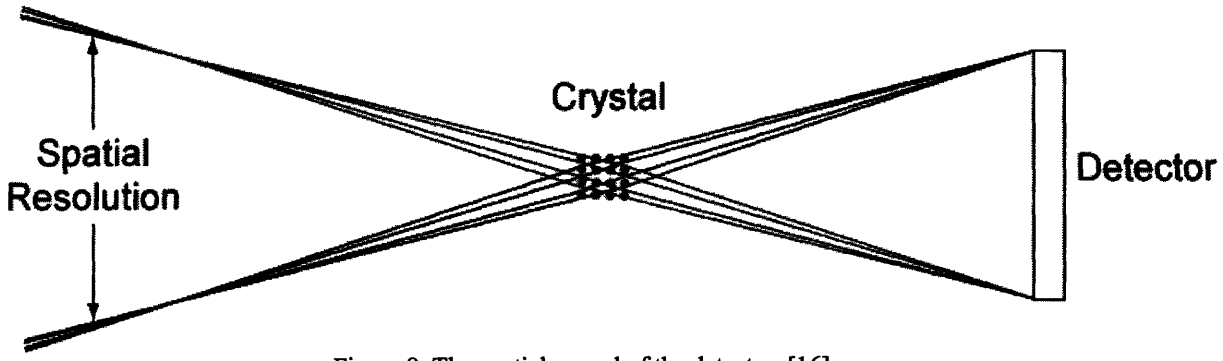

Figure 8. The spatial spread of the detector. [16]

The importance of this geometry is that a source on the Rowland circle will be focused to a single point still on the Rowland circle.

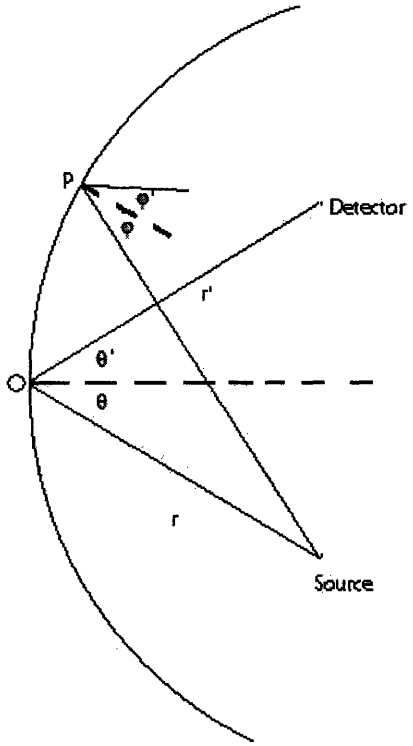

Figure 9. Multiple rays from source to detector on the Rowland circle arrangement. The curve shown is curve of the crystal. Figure not drawn to scale.

Let the coordinates of the source be $S(x_0, y_0)$, and the coordinates of the detector $D(x_1, y_1)$. In addition, allow that $y_0^2 + (x_0 - R/2)^2 = (R/2)^2$, so the source lies on the Rowland circle. The point O is centered at (0, 0) and the point $P(x_2, y_2)$ is assumed as a random point of reflection.

The lines from the source to points O and point P are described by the equations, given by geometrical reasoning,

$$\overline{SO}: y = \frac{y_0}{x_0} x \ , \tag{11}$$

and

$$\overline{SP}: y - y_2 = \frac{y_0 - y_2}{x_0 - x_2}(x - x_2). \tag{12}$$

These lines have slopes (y_0/x_0) and $(y_0-y_2)/(x_0-x_2)$, respectively. The equations describing the circle are

$$y = \pm\sqrt{R^2 - (x-R)^2} \ , \tag{13}$$

$$\frac{dy}{dx} = \mp\frac{x-R}{\sqrt{R^2-(x-R)^2}}. \tag{14}$$

At points O and P, assumed to be in the positive half of the circle, the slope of the tangent line to the circle is ∞ and $-(x_2-R)/(R^2-(x_2-R)^2)^{(1/2)}$, respectively. The incident lines are reflected from this tangent line, and from spectroscopic arguments, the angle of incidence is equal to the angle of reflection, since there is no change in the material of propagation after reflection. The tangent of the line is related to the angle from the x-axis by m = tan (A), where m is the slope and A is the angle from the X-axis. If the slope of the tangent line to the circle is at angle α and the angle of the line from the source to the circle, referenced to the axis, is at angle β, then the slope of the reflected line is $2\alpha - \beta$; see Appendix A for picture and details. Using this argument, the equations of the two reflected lines are found to be

$$y_{R1} = -\frac{y_0}{x_0} x \ , \tag{15}$$

$$y_{R2} - y_2 = \tan\left[2\tan^{-1}\left(-\frac{x_2 - R}{\sqrt{R^2 - (x_2 - R)^2}}\right) - \tan^{-1}\left(\frac{y_0 - y_2}{x_0 - x_2}\right)\right](x - x_2). \quad (16)$$

Using trigonometric identities on equation 16 provides a simplified form of the equation

$$y_{R2} - y_2 = -\frac{2(x_2 - R)(x_0 - x_2)\sqrt{R^2 - (x_2 - R)^2} + R^2(y_0 - y_2)}{2(x_2 - R)(y_0 - y_2)\sqrt{R^2 - (x_2 - R)^2} + R^2(x_0 - x_2)}(x - x_2). \quad (17)$$

The focus point occurs when the lines y_{R1} and y_{R2} cross. Combining equations 15 and 17, the focus point's coordinates are found to be

$$x_f = \frac{\frac{2(x_2 - R)(x_0 - x_2)\sqrt{R^2 - (x_2 - R)^2} + R^2(y_0 - y_2)}{2(x_2 - R)(y_0 - y_2)\sqrt{R^2 - (x_2 - R)^2} + R^2(x_0 - x_2)}x_2 + y_2}{\frac{2(x_2 - R)(x_0 - x_2)\sqrt{R^2 - (x_2 - R)^2} + R^2(y_0 - y_2)}{2(x_2 - R)(y_0 - y_2)\sqrt{R^2 - (x_2 - R)^2} + R^2(x_0 - x_2)} - \frac{y_0}{x_0}}, \quad (18)$$

$$y_f = -\frac{y_0}{x_0}\frac{\frac{2(x_2 - R)(x_0 - x_2)\sqrt{R^2 - (x_2 - R)^2} + R^2(y_0 - y_2)}{2(x_2 - R)(y_0 - y_2)\sqrt{R^2 - (x_2 - R)^2} + R^2(x_0 - x_2)}x_2 + y_2}{\frac{2(x_2 - R)(x_0 - x_2)\sqrt{R^2 - (x_2 - R)^2} + R^2(y_0 - y_2)}{2(x_2 - R)(y_0 - y_2)\sqrt{R^2 - (x_2 - R)^2} + R^2(x_0 - x_2)} - \frac{y_0}{x_0}}. \quad (19)$$

The distance from this point to the point (R/2, 0) is R/2. This distance is the same as the distance from the point (x_0, y_0) to the point (R/2, 0). Therefore, the rays from a source on the Rowland circle is focused to another point on the Rowland circle. It can also be found, by following arguments about the path difference between the two rays, that only certain discrete wavelengths of light have constructive interference at various points on the Rowland circle, which provides this geometry's spectral differentiation properties. [17]

Overall, the Johann configuration allows high signal at the detector and measuring a range of spectral lines at the same time, and it was used at the National Spherical Torus

Experiment (NSTX) [5]. The estimated resolution of the detector at NSTX was $\lambda/\Delta\lambda = 6000$. In general, spherically bent crystals have been found to be much more effective line measurements than cylindrical crystals, and their use is preferable for the measurements required of NeSoXs. [18]

7. NeSoXs I

Based on the Johann configuration and the inclusion of neon in the Alcator gas puffing impurity injection system, the spectrometer used in the Hanbit experiment in Korea was brought to and installed on Alcator C-Mod.

a. Design and Arrangement

The NeSoXs design consisted of a central chamber attached to the Alcator vessel and a CCD camera (Princeton Instruments LCX-TE/CCD-1242-HER). A diagram of the NeSoXs spectrometer is shown in Figure 10.

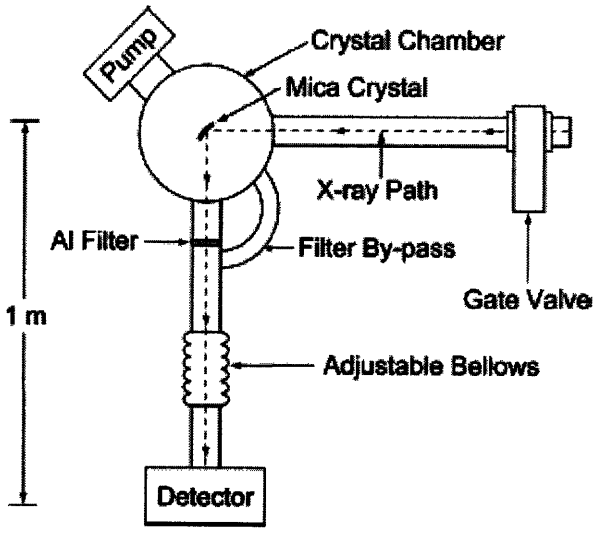

Figure 10. NeSoXs arrangement with respect to the Alcator vacuum vessel. [10]

The spectrometer was designed with several considerations. First, due to the nature of the X-rays studied and vacuum requirements on Alcator, using a vacuum window is not possible and any air that leaks into the chamber attenuates the X-rays. These two issues, particularly Alcator regulations on opening gate valves to the chamber, force the use of high vacuum components. The pressure was kept to a maximum of 10^{-6} Torr for almost the entire operational time of NeSoXs. Second, the crystal had to be held at a proper distance from the detector and at the correct angle. This was accomplished by an adjustable camera arm and properly aligned ports on the crystal chamber. The plasma to crystal distance was ignored, because there is no reasonable way to move the spectrometer to the proper distance of the plasma since there are physical constraints from the Alcator vacuum vessel. Third, the plasma emits a large amount of radiation in the visible range. Since CCD cameras are efficient at picking up visible radiation, a thin (~100 nm) aluminum filter had to be included in the camera arm, to avoid blooming the CCD. Fourth, the camera requires water-cooling to support its Peltier cooling system. The Peltier cooling system cools the internal part of the camera to -40°C, and transfers the removed heat from the CCD chip to a heat sink. This heat sink has to be cooled externally, or there is a risk of damage to the camera.

During operation, the camera controller receives triggers from an external source to start acquisition. Software was running on the computer controlling the camera that automatically prepares the computer for receiving the triggers and stores the received data and camera parameters in the CMOD tree (the data storage system for Alcator using MDSPlus).

b. Results

NeSoXs proved capable of seeing most of the elemental lines predicted by theory, and was able to identify iron in the plasma despite its presence not being expected. A serendipitous

fluorine line is present in nearly all of the discharges from the Alcator plasma, which allows NeSoXs to operate with diminished efficiency during runs where neon is not introduced into the plasma.

The camera can operate in several regimes. The simplest one is allowing the CCD accumulate charge for the entire plasma discharge and then reading out the entire chip. This method produces pictures such as the one shown in Figure 11.

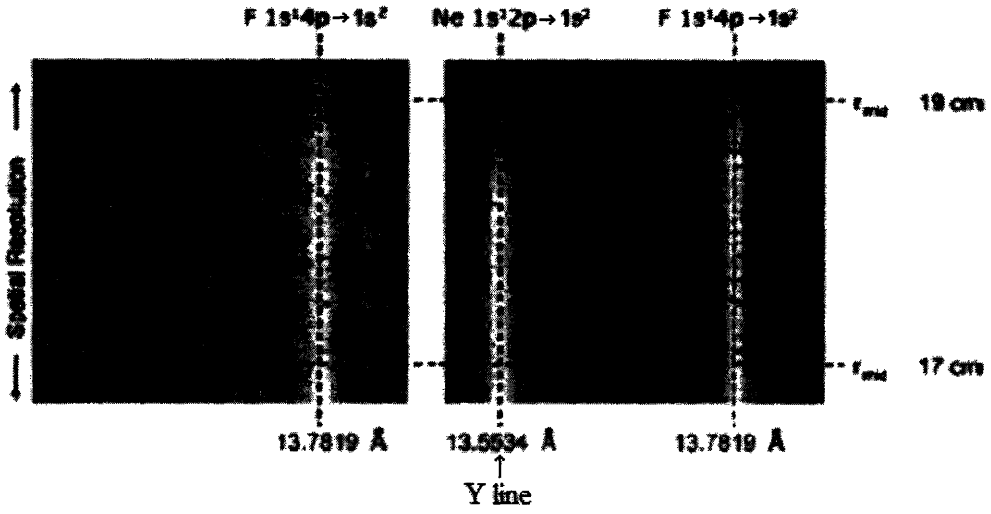

Figure 11. Standard full frame spectra from discharges with neon (right) and without neon (left). [10]

Analyzing the pictures produced, line plots were created that show counts versus wavelength at a certain spatial position; one such plot is shown in Figure 12.

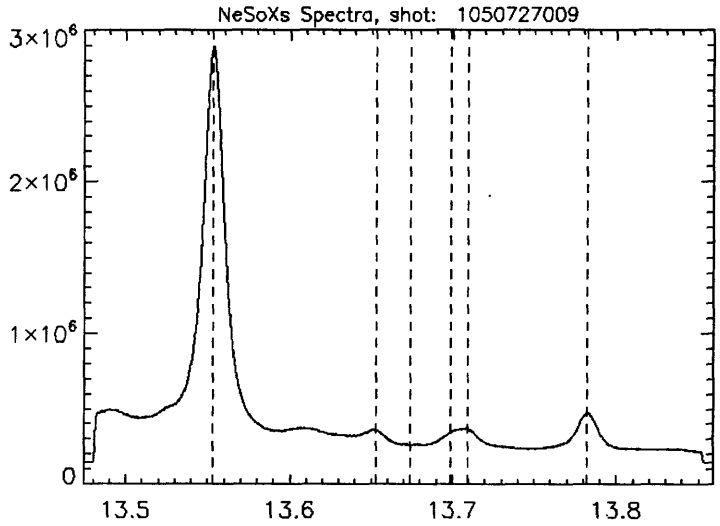

Figure 12. Line out from NeSoXs from a neon containing discharge. The Y-axis is measured in arbitrary units of intensity and X-axis is in Angstroms. Dotted lines show probable lines, and the large peaked line is the neon Y line.

The full frame readout, however, takes approximately a minute, so it is not feasible for measuring temporal changes in the plasma. This forces the use of regions of interest (ROI) to speed up the readout of the CCD. These are regions that are read and stored in memory; the other regions are discarded. The ROIs are chosen to select either an array of spatial coordinates or a wide spectral range. Two commonly used ROI arrangements are shown in Figure 13. The camera controller manual provides an equation to find the readout rate of the camera; however, this equation was found to provide only an order of magnitude estimate. The readout is confounded by how fast the camera receives triggers, and the computer and CMOD tree storage time. In general, the fastest readout that was possible was 90 frames over two seconds for small ROIs. At this rate, the spectral data were too blurred to be valuable, so most often around 30 frames were taken during the two-second plasma discharges.

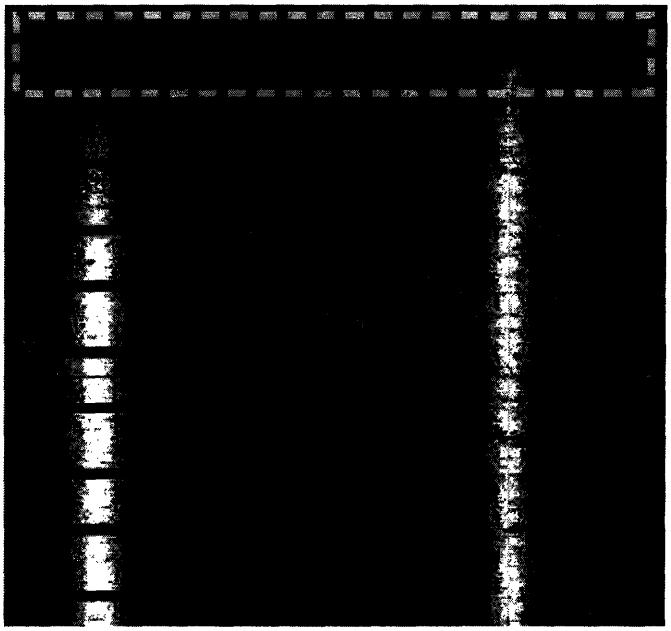

Figure 13. NeSoXs full-frame spectrum with two commonly used ROIs overlayed. The gray rectangle represents a full spectral analysis used to provide line graphs such as the one in Figure 12. The black rectangle represents multiple spatial analyses for neon, intended to provide poloidal rotation analysis. [10]

NeSoXs was also able to provide brief time histories of spectra from the plasma, one of which is shown in Figure 14. Due to the iron injection in this shot, it was possible to estimate the impurity confinement time as $\tau = 57$ ms.

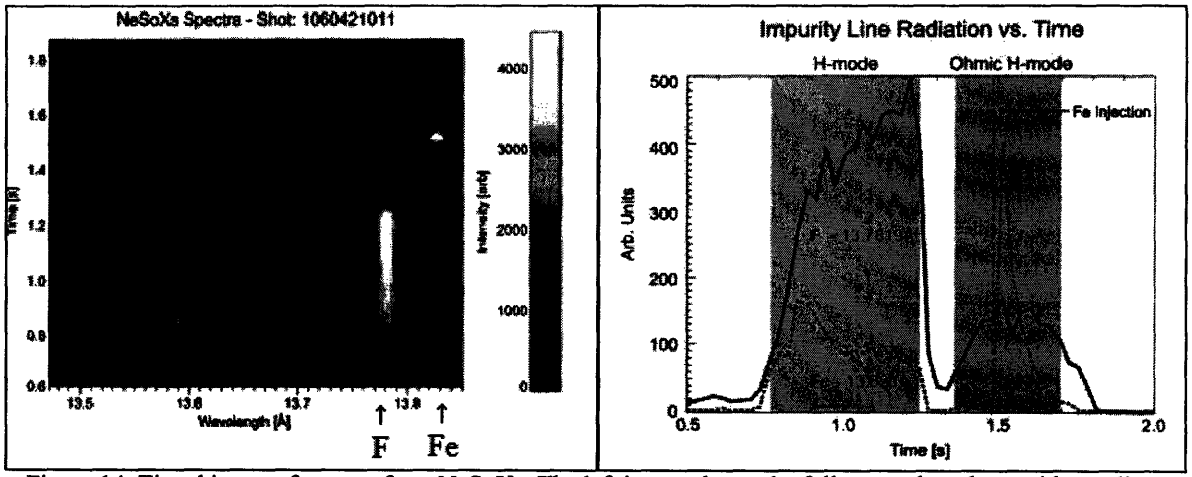

Figure 14. Time history of spectra from NeSoXs. The left image shows the full spectral readout, with two lines marked, while the right frame shows the intensity of those two lines. [10]

c. Other Issues

Several important factors arose during the construction, calibration, and debugging of NeSoXs. The first of these factors was the amount of time necessary to pump out the vacuum chamber. Most of the connections on the experiment were O-ring connections and the vacuum chamber was far too large for its intended task, so it required a bakeout (heating the chamber to 40°C) and nearly a week to lower the pressure to 10^{-6} Torr during the first pump down. During subsequent exposures to atmosphere, it took about a day to pump the chamber out to the same level. The second issue was shock waves. During the first construction of NeSoXs, the camera gate valve was accidentally opened to atmosphere while the camera was under vacuum. This caused a shock wave to the CCD, resulting in its charge accumulator being displaced. The third issue was the difficulty of positioning the crystal and chamber relative to the plasma. Repositioning the crystal in the chamber required exposing the chamber to atmosphere and opening the crystal chamber, which would be extremely time consuming. Furthermore, there were problems with the aluminum filter, since its alignment is important and small pressure differences can destroy it. The long filter bypass seen in Figure 10 exists to maintain pressures on both sides of the filter.

The last issue was damage to the mica crystal. Upon removing NeSoXs from the Alcator cell, a discoloration was noticed on the crystal. This discoloration was determined to be the mica crystal ungluing itself from its glass backing. Most likely this is due to an imperfection in the crystal; unfortunately, it rendered a third of the crystal unusable.

8. NeSoXs II Design

a. Motivation and Criteria

The bulk of this project was designing and constructing the Neon Soft X-ray Spectrometer upgrade, or NeSoXs II, which was conceived as a way of achieving the goals of the original NeSoXs and remedying several of its problems. NeSoXs II was given a better plasma view and a superior camera (Princeton Instrument PI-SX) than its predecessor's camera. A new mica crystal was obtained to replace the damaged one. The design also had to be far more compact and dynamic than the previous one was, in order to allow for a wider range of motion and position adjustment. The port where NeSoXs II is placed, the same one as NeSoXs, has become far more crowded than it was previously, so the compactness of the spectrometer became extremely important.

b. The Design

The mechanical design was completed using the Solid Edge software, which allowed three-dimensional manipulation of the spectrometer parts and details. It also allowed placing the spectrometer on a model of the port where NeSoXs II is positioned. The final model of the completed spectrometer is shown in Figure 15. All important design decisions will be discussed in this section.

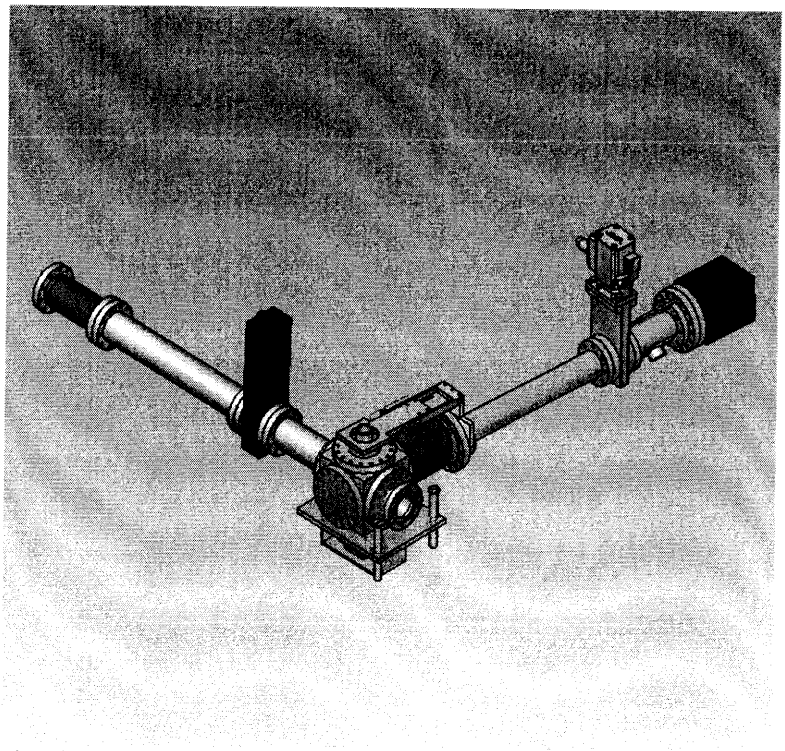

Figure 15. Isometric drawing of NeSoXs II. The black vertical object on the left is a 4 5/8" gate valve, and the clear object below the cube is the apartment for the rotation stage.

The first design decision was to construct the chamber out of primarily stainless steel with copper gaskets between the individual parts, in order to make it ultra high vacuum compatible. This would further lower vacuum pumping times and improve the vacuum quality in the chamber, although this increased the difficulty of assembly and spectrometer weight.

The torus arm, shown on the left of the Figure 15, was constructed from 4 5/8" Conflat vacuum parts (most were ordered from MDC vacuum). Flanges with a 4 5/8" nominal size have a maximum internal diameter of 3" (NeSoXs used 4.5" nominal flanges with a maximum internal diameter of 2.5"), lowering the chance of the sides of the tube impinging on the rays from the plasma to the crystal, thus lowering throughput. Analyzing the spread of the rays from the spherically bent mica crystal, it was found there is sufficient safety to allow a wide range (~ ±2") of motion for the crystal chamber and still not be vignetted by the sides of the torus arm or

port flange. The first flange occurs where the torus arm ends and the port flange begins, and the second flange is where the 10" extension from the port ends.

The vignetting question can be resolved by following geometric calculations derived from the discussion in section 6.b.iii. Since the only photons of interest are those that will impinge on both the detector and the crystal, it is possible to imagine that the detector is generating rays, which then enter the plasma. These rays define a maximum figure, a rectangle, within which any emission from the plasma will fall on the detector. The vertical length of the rays from the crystal spreads at approximately 1.5°. This angle was found by calculating the angle pitch of the ray from the bottom of the CCD to the top of the crystal. Therefore, the equation of the height of this rectangle, assuming no spectrometer pitch, is

$$H = C_H + 2\tan(1.5^\circ)x, \tag{20}$$

where C_H is the crystal height and x is the distance from the crystal. The width of the rectangle takes into account the horizontal focus that occurs at the Rowland circle. This means that the horizontal width at 104 cm from the crystal must have the same size as the CCD width, 2.6 cm. This fixes the angle that the rays follow, and the equation of the width of the rays, assuming no spectrometer pitch, is

$$W = CCD_W + \frac{(C_W - CCD_W)}{R}(R - x), \tag{21}$$

where C_W is the crystal width times the cosine of its orientation towards the plasma, ~45° for NeSoXs II, CCD_W is the CCD width, and R is the distance to the Rowland circle from the crystal, 104 cm. The spectrometer can undergo some vertical movement, so these equations need to be adjusted for those changes. The angles will be at most ±5°, so this does not affect the equations a great deal, and this position ability was taken into account during simulations of the rays.

In Figure 16, the maximum spread of these rays is shown in relation to the flanges that the beam goes through. This Figure assumed a 1° upward pitch for the spectrometer.

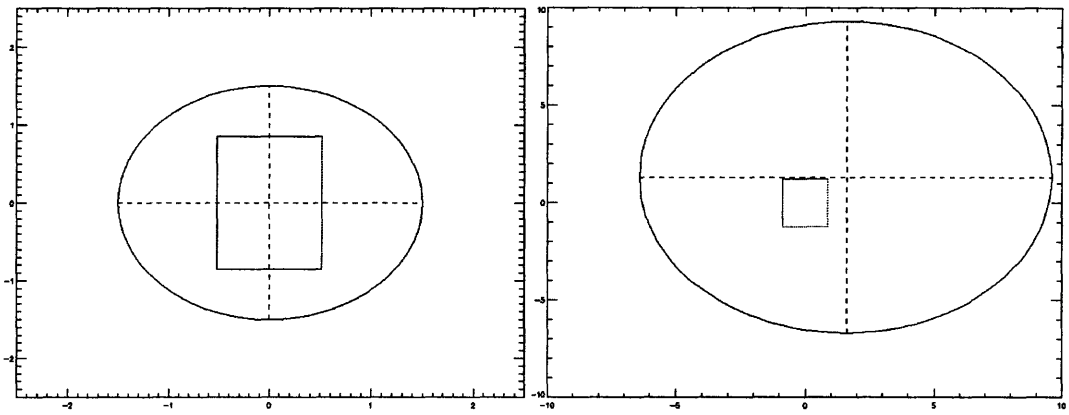

Figure 16. The ray trace of where the view of spectrometer falls in the near 4 5/8" flange (left), and the far 10" flange (right).

It is important to note that the port flange has a 1° downward facing 4 5/8" flange for NeSoXs II, so the neutral position for the spectrometer has a slight upwards angle. Additional characteristics of the torus arm include a hinged bellows directly at the K-port flange, the pneumatically controlled gate valve, and a ceramic electrical break (not shown in figure) from the tokamak.

The torus arm connects directly to a 6" welded cube, which acts as the crystal chamber. The face where the torus arm attaches has been named the forward face of the cube. The left side of the cube has to be blanked off for accessibility issues to the port. The back face attaches to the turbo and roughing pump via a second electrical break. These are auxiliary systems, so they have not been shown. The bottom of the cube sits inside the vertically positioning system, which was named the apartment, shown in Figure 17.

The apartment uses two .75" coarse threaded lengths of threaded rod to support the apartment and cube on the stand below the spectrometer. The apartment also houses the rotation stage for the crystal assembly. Because of difficulties with positioning the crystal in the original NeSoXs, an OptoSigma SGSP-60YAW motorized rotation stage was purchased to provide

computer control of the crystal angle. The rotation stage attaches to a post that is screwed into the crystal holder through a vacuum quick disconnect (MDC 412003). Finally, the apartment can attach directly to the cube, stopping it from moving and putting strain on the rotation stage.

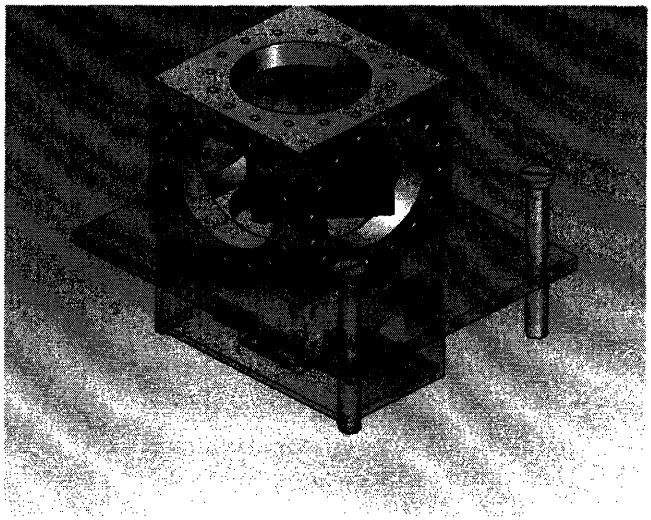

Figure 17. Isometric view of NeSoXs II apartment and cube. Apartment material is aluminum, and the black part inside the cube is the crystal holder.

The upper section of the cube attaches to the chamber pressure gauges. This section also is important because it provides the support for the yoke piece. Due to the required angle from crystal being 104°, the pivot point for the camera arm needs to be directly on top of the crystal as opposed to three inches away as it would be, since the bellows attaches to the side of the cube. This requires the use of a device that will compress the bellows slightly on one side, thus moving the pivot point back to the center of the cube. The yoke also provides a measure of adjustability for the length of the camera arm, and it stops the bellows from collapsing from the difference in pressure of the atmosphere and internal pressure of the chamber. The yoke model is shown in Figure 18; it is constructed of thick plates of aluminum and screws into the top half of the 6" camera arm bellows.

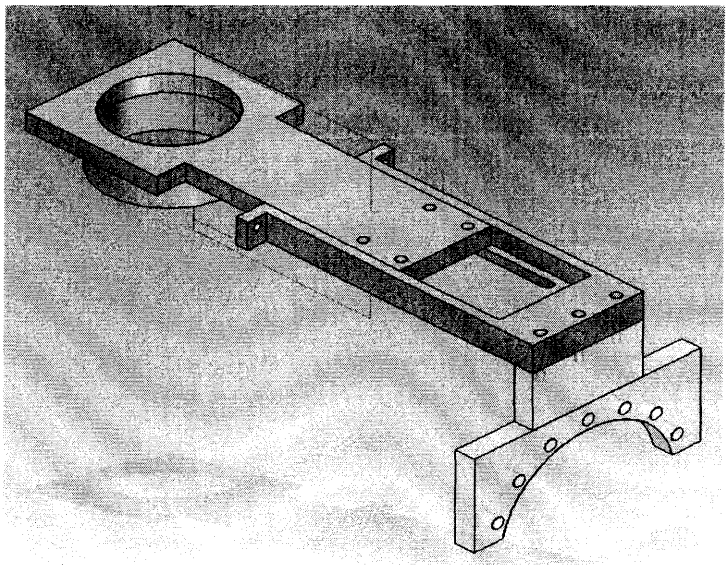

Figure 18. Model of the yoke for the NeSoXs II camera arm.

As mentioned before, the yoke attaches to the camera arm, which is located on the right face of the cube. This arm consists of a 6" bellows that reduces to a 4.5" tube and attaches to the camera gate valve. On the camera side of the crystal the rays focus to the camera, so it is safe to build it with 4.5" nominal flanges (2.5" nominal ID) without risking the rays impinging on the tube walls. Beyond the camera gate valve is the camera assembly, which will be discussed in more detail later in this section.

An important part immediately after the 6" bellows is the filter holder. In order to avoid bulky and ineffective bypasses the filter holder was designed as a stand-alone piece with its schematic shown in Figure 19. The filter holder is a 4.5" double sided blank, with a specific form machined into it. The filter attaches to one of its sides and a blank thin piece of aluminum on standoffs attaches to the other. The slots in the filter act as bypasses for the air in the camera arm to escape and not rupture the filter, and the blank stops light from escaping through the bypasses.

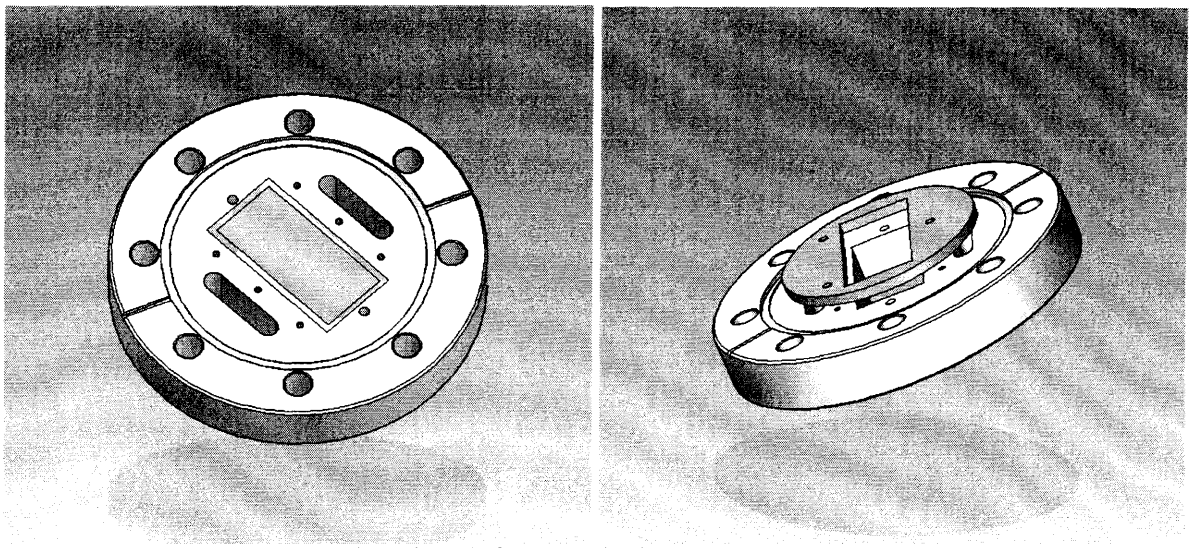

Figure 19. Filter holder assembly views front (left) and back (right). The filter holder is seen in the front view, while the blank is seen in the back view. The six regularly spaced holes around the rectangular section are for attaching the filter and blank; all other holes are bypasses.

The final section of the camera arm is the CCD camera and its assembly. This section has a 4.5" gate valve in order to seal it from the rest of the chamber, which allows it to be removed from the rest of the spectrometer. This section also has its own pressure gauges and leak valve, to avoid possible shock waves from opening the gate valve prematurely. The leak valve also allows steady re-pressurization of the camera for long storage periods.

The final section of interest is the stand and the way it attaches to the spectrometer. The stand is required to support the spectrometer weight at the two threaded rods and at the camera side. This supports the spectrometer under the threaded rods, the camera, and at the hinge. In addition, a positioning system on the camera side is required to stop the camera arm from swinging back towards 0° from the right face of the cube. The stand was built out of two 4"x3" aluminum I-beams, with a twelve-inch square base plate bolted to the grating of the Alcator cell. Two 1" aluminum rails extend the I-beam out to under the threaded rod supports, and a G10 plate assembly with several positioning screws provides the horizontal camera side positioning.

A G10 block provides the support under the camera side. In Figure 20, the entire assembly is shown on the Alcator port in relation to selected other diagnostics.

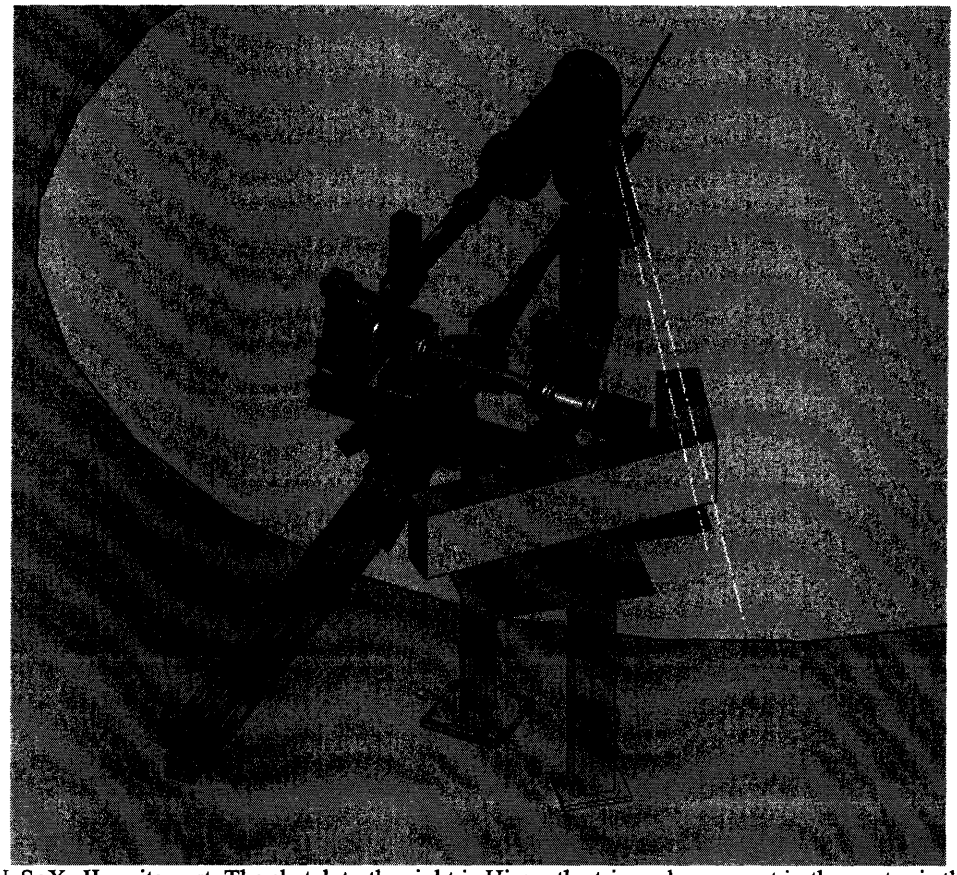

Figure 20. NeSoXs II on its port. The sketch to the right is Hirex, the triangular support in the center is the Hirex JR support, and the device under NeSoXs is the Surface Science station.

c. Spectrometer View and Predictions

NeSoXs II has a radically different view of the plasma than the one NeSoXs had. It is located approximately 20 cm above the midplane of the plasma, while NeSoXs was located below the midplane, and NeSoXs II can undergo angular positioning, with an expected upward angle of 1°. This view of the plasma is shown in Figure 21.

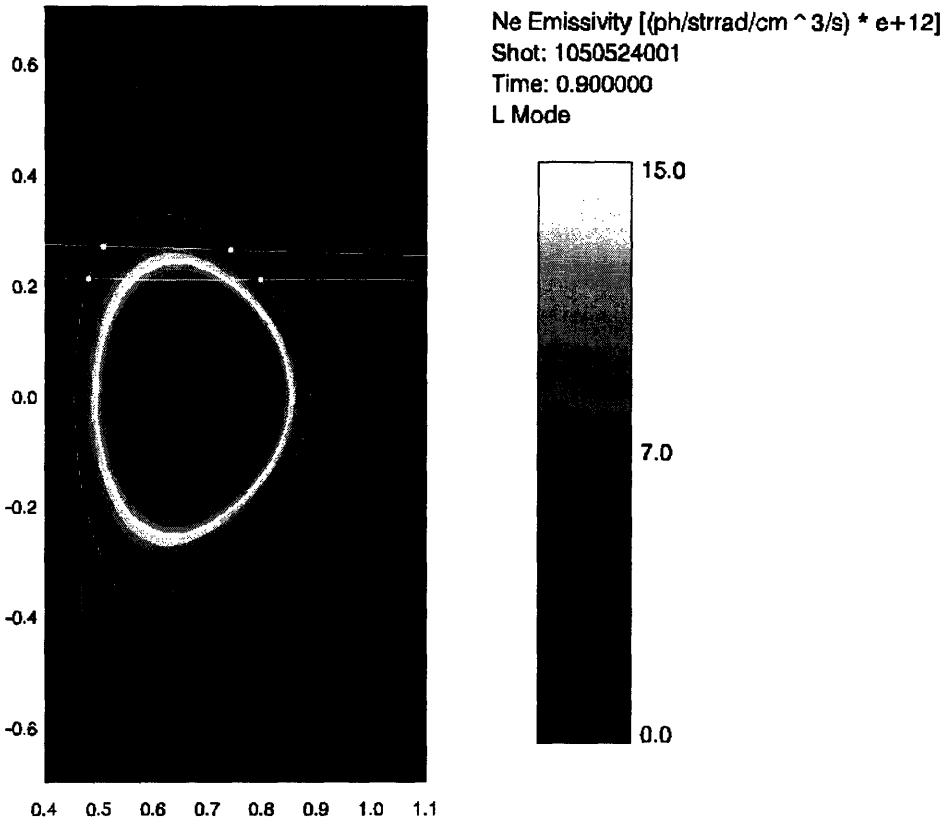

Figure 21. NeSoXs II plasma view on neon emissivity plot from a typical discharge.

It is seen that the view of the spectrometer is expected to pass through the brightest section of the plasma for the analyzed discharge. This plasma is relatively representative of the types that are created at Alcator, so the spectrometer should be at the ideal location for signal.

Exact signal will depend on the temperature, density, magnetic field lines, and spectrometer efficiency, but a rough estimate of the photons seen at the CCD can be performed. The average emissivity of the neon within the span of the spectrometer view is 12 $*10^{12}$ photons/ (steradian * cm^3 * s). The volume of this box is given by the values found from equations 20, 21, and an effective depth of ~20cm. The average area of the rectangle of interest is ~30 cm, which corresponds to approximately .00128 sterradian, assuming that every emitting atom sees the same rectangle, which is only valid for the rough estimate that is being performed. This calculation leads to an approximate number of photons seen from neon of $9.2*10^{12}$, assuming no

other losses in the system. The CCD, however, does not register individual photons; it records the amount of charge collected, which has a complicated relation to the photons impinging on the detector. The CCD photon to count ratio can be found by analyzing the counts in a non-line containing region of the CCD and by analyzing a line that is seen by other spectrometers, such as the xenon line. In general, it is expected that NeSoXs II will have similar signal to NeSoXs with improvements due to its superior vacuum chamber and better positioning capabilities.

9. Conclusion

a. Status and Discussion

The Neon Soft X-ray Spectrometer upgrade has been built and is in the process of being installed on Alcator. The total assembly weighs approximately 150 lbs; pictures of the completed spectrometer are included in Appendix B. The crystal was aligned and a pump down test was performed. Ten minutes after the turbo pump activation on a chamber never exposed to vacuum, the pressure had fallen from 2 Torr to $6.2\times10^{(-5)}$ Torr, which is a pressure the previous chamber required a bakeout to achieve. Visual inspection of the filter shows that the filter worked successfully. The crystal alignment was also a success with the crystal reflected a beam within 1 mm of the emission point that is 2m away.

b. Future Work

Due to unexpected interferences with the Surface Station and Hirex JR, the stand is undergoing a brief redesign in order to account properly for its new location and different weight distribution. Upon installation in the cell, the majority of the pre-existing software and data analysis software can be re-used. After the data acquisition is operational, the chamber will be positioned to view the edge of the neon line visible to provide a reference for measurements, and from the Doppler shift visible in the lines, a poloidal rotation velocity of the plasma will be

calculated. Using the plasma modeling code, EFIT [19], it will be possible to run reconstructions of the plasma magnetic field lines, temperature, and density. Knowing these values and the emission spectra seen by NeSoXs II, atom density as a function of radius can be found. Finally, by finding the line width of the neon line, the temperature of the impurity can be found, and this tends to be close to the ion temperature.

References

[1] I.H. Hutchinson, R. Bovin, F. Bombarda, P. Bonoli, S. Fairfax, C. Fiore, J. Goetz, S. Golovato, R. Granetz, M. Greenwald, S. Horne, A. Hubbard, J. Irby, B. LaBombard, B. Lipschultz, E. Marmar, G. McCracken, M. Porkolab, J. Rice, J. Snipes, Y. Takase, J. Terry, S. Wolfe, C. Christensen, D. Garnier, M. Graf, T. Hsu, T. Luke, M. May, A. Niemczewski, G. Tinios, J. Schachter, H. Urbahn. "First results from Alcator-C-Mod*." Physics of Plasmas. Vol. 1 Issue 5, May. p 1511 – 1518. 1994.

[2] F. Wagner, G. Becker, K. Behringer, D. Campbell, A. Eberhagen, W. Engelhardt, G. Fussmann, O. Gehre, J. Gernhardt, G. v. Gierke, G. Haas, M. Huang, F. Karger, M. Keilhacker, O. Klüber, M. Kornherr, K. Lackner, G. Lisitano, G. G. Lister, H. M. Mayer, D. Meisel, E. R. Müller, H. Murmann, H. Niedermeyer, W. Poschenrieder, H. Rapp, H. Röhr, F. Schneider, G. Siller, E. Speth, A. Stäbler, K. H. Steuer, G. Venus, O. Vollmer, and Z. Yü. "Regime of Improved Confinement and High Beta in Neutral-Beam-Heated Discharges of the ASDEX Tokamak." Physical Review Letters. Vol. 49, Num. 19, Nov. p. 1408 – 1412. 1982.

[3] D. L. Robbins, H. Chen, P. Beiersdorfer, A. Ya. Faenov, T. A. Pikuz, M. J. May, J. Dunn, A. J. Smith. "A high-resolution compact Johann crystal spectrometer with the Livermore electron beam ion trap." Review of Scientific Instruments. Vol 75. April. p 3717-3719. 2004.

[4] I. H. Hutchinson. Principles of Plasma Physics: Second Edition. Cambridge University Press: Cambridge, UK. ©2002.

[5] M. Bitter, K.W. Hill, A. L. Roquemore, P. Beiersdorfer, S. M. Kahn, S. R. Elliot, B. Fraenkel. "Imaging x-ray crystal spectrometers for the National Spherical Torus Experiment." Review of Scientific Instruments. Vol 70, Num 1, Jan. p 292 – 295. 1999.

[6] S. G. Lee, S. M. Hwang, and M. Bitter. "X-ray crystal spectrometer for the HANBIT mirror machine." Review of Scientific Instruments. Vol. 70, Num 1, Jan. p 299 – 301. 1999.

[7] D.J. Griffths. Introduction to Quantum Mechanics: Second Edition. Pearson Education: Upper Saddle River, New Jersey. ©1995

[8] A. Ince-Cushman. Personal Communication. April 07, 2007.

[9] R.A. Hulse. Nucl. Tech. Fus. 3 (1983) 259.

[10] A. Ince-Cushman, J. E. Rice, S. G. Lee, M. Bitter, M. Reinke, Y. Podpaly. "Preliminary results from the soft x-ray crystal spectrometer on Alcator C-Mod." Review of Scientific Instruments. Vol 77, 2006.

[11] R. J. Groebner, K. H. Burrell, R. P. Seraydarian. "Role of Edge Electric Field and Poloidal Rotation in the L-H Transition." Physical Review Letters. Vol. 64, Num 25, June. p. 3015 – 3018. 1990.

[12] K. Lukin. "Bragg's Law and Diffraction: How waves reveal the atomic structure of crystals." Center for High Pressure Research SUNY Stony Brook. Available HTTP: http://www.eserc.stonybrook.edu/ProjectJava/Bragg/

[13] H. H. Johann, Z. Phys. 69, 185 (1931).

[14] S. G. Lee, J. G. Bak, Y. S. Jung, M. Bitter, K. W. Hill, G. Hölzer, O. Wehrhan, and E. Förster. "An efficient method for simultaneous measurement of the integrated reflectivity of crystals in multiple orders of reflection using the bremsstrahlung continuum from an x-ray tube and comparison of experimental results for mica with theoretical calculations." Review of Scientific Instruments. Volume 74 Number 12. December 2003. pp 5046 – 5052.

[15] M. Bitter, G. Bertschinger, W. Biel, G. Fuchs, S. von Goeler, H.-J.Kunze, D. Rusbüldt, and J. Weinheinmer. "Spatially Resolved Spectra of ArXVI and ArXVII from a New Type of Imaging X-Ray Crystal Spectrometer at TEXTOR-94" ECA Vol.23J. 1999 pp 1689 – 1692.

[16] A. Ince Cushman, J. E. Rice, M. Reinke, M. Bitter. "Imaging High Resolution X-ray Spectroscopy: A Swiss Army Knife of a Tokamak Diagnostic". PhD Seminar. May 8, 2006

[17] Hendrik Gideon Van Zyl. Master's Thesis titled, "Modelling of Integrated Optic Components for Lightwave Communications Systems using the Beam Propagation Method." Rand Afrikaans University. July 2001.

[18] L. M. Belyaev, A. B. Gil'varg, Yu. A. Mikhailov, S. A. Pikuz, G. V. Sklizkov, A. Ya. Faenov, and S. I. Fedotov. "High-luminosity x-ray spectrograph with a spherically bent crystal analyzer, designed for laser plasma diagnostics." Soviet Journal of Quantum Electronics. Volume 7 Number 1 January. 1977. pp 67-70.

[19] Lao, L.L., StJohn, H., Stambaugh, R.D., Kellman, A.G., Pfeiffer, W., "Reconstruction of Current Profile Parameters and Plasma Shapes in Tokamaks," Nucl. Fusion 25 (1985) 1611.

Appendix A

Assuming that two lines intersect and have angles A and B from the horizontal axis, it is possible to find the angle of reflection of on of the lines from the other. The diagram of this arrangement is shown in Figure A.1. Using triangle angle summation and parallel line relations, it is found that the reflected line is at the angle (B-2A) from the horizontal axis.

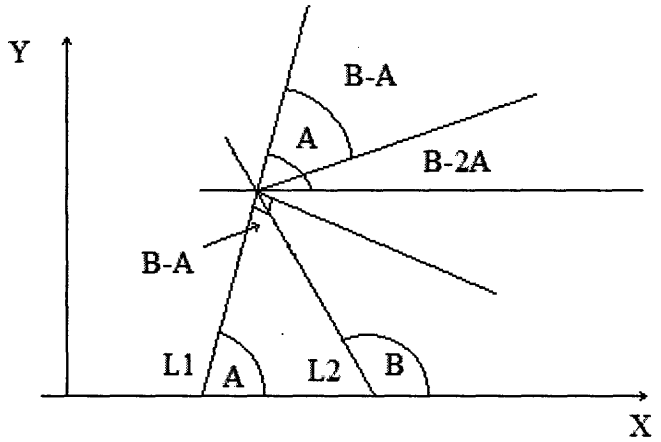

Figure A.1. Intersection of two lines with the line L2 being reflected from the line L1. The angle of the reflected line from the horizontal is found to be B-2A.

Appendix B

The following are pictures of the Neon Soft X-ray Spectrometer in the set-up lab.

Figure B.1. Picture of the NeSoXs II crystal chamber. The arm shown is the camera arm.

Figure B.2. Picture of NeSoXs II showing the chamber pumps, and camera arm. Camera is not attached to avoid possible damage.

Blank Page